Research Article | Vol. 26, No. 21 | 15 Oct 2018 | OPTICS EXPRESS 27014
Optics EXPRESS

Mid-infrared cavity resonator integrated grating filters

S. Augé,[1] S. Gluchko,[2] A.L. Fehrembach,[3] E. Popov,[3] T. Antoni,[4] S. Pelloquin,[1] A. Arnoult,[1] A. Monmayrant,[1,*] and O. Gauthier-Lafaye[1]

[1]*LAAS-CNRS, Université de Toulouse, CNRS, Toulouse, France*
[2]*Laboratoire EM2C, CNRS, CentraleSupélec, Université Paris-Saclay, 3, rue Joliot Curie, 91192 Gif-sur-Yvette cedex, France*
[3]*Aix-Marseille Univ, CNRS, Centrale Marseille, Institut Fresnel, Marseille, France*
[4]*Laboratoire de Photonique Quantique et Moléculaire, CentraleSupélec, ENS Paris-Saclay, CNRS, Université Paris-Saclay, Grande Voie des Vignes, 92290 Châtenay-Malabry, France*
[*]*antoine.monmayrant@laas.fr*

Abstract: Cavity Resonator Grating Filters (CRIGFs) working in the Mid-Infrared are reported, with narrow-band resonant reflectivity peaks around 2200 cm^{-1} (4.6 μm). They are fabricated in the GaAs/AlGaAs material system that can potentially cover the whole [1-12] μm spectral range. TE-polarized peak reflectivity is 30% with a 4 cm^{-1} full width at half maximum.

References

1. K. Kintaka, T. Majima, J. Inoue, K. Hatanaka, J. Nishii, and S. Ura, "Cavity-resonator-integrated guided-mode resonance filter for aperture miniaturization," Opt. Express **20**, 1444–1449 (2012).
2. S. Tibuleac and R. Magnusson, "Reflection and transmission guided-mode resonance filters," J. Opt. Soc. Am. A **14**, 1617–1626 (1997).
3. R. Laberdesque, O. Gauthier-Lafaye, H. Camon, A. Monmayrant, M. Petit, O. Demichel, and B. Cluzel, "High-order modes in cavity-resonator-integrated guided-mode resonance filters (crigfs)," J. Opt. Soc. Am. A **32**, 1973–1981 (2015).
4. N. Rassem, A.-L. Fehrembach, and E. Popov, "Waveguide mode in the box with an extraordinary flat dispersion curve," J. Opt. Soc. Am. A **32**, 420 (2015).
5. X. Buet, E. Daran, D. Belharet, F. Lozes-Dupuy, A. Monmayrant, and O. Gauthier-Lafaye, "High angular tolerance and reflectivity with narrow bandwidth cavity-resonator-integrated guided-mode resonance filter," Opt. Express **20**, 9322–9327 (2012).
6. K. Kintaka, K. Shimizu, Y. Kita, S. Kawanami, J. Inoue, S. Ura, and J. Nishii, "Potential characterization of free-space-wave drop demultiplexer using cavity-resonator-integrated grating input/output coupler," Opt. Express **18**, 25108 (2010).
7. S. Ura, K. Shimizu, Y. Kita, K. Kintaka, J. Inoue, and Y. Awatsuji, "Integrated-optic free-space-wave coupler for package-level on-board optical interconnects," IEEE J. Sel. Top. Quantum Electron. **17**, 590–596 (2011).
8. X. Buet, A. Guelmami, A. Monmayrant, S. Calvez, C. Tourte, F. Lozes-Dupuy, and O. Gauthier-Lafaye, "Wavelength-stabilised external-cavity laser diode using cavity resonator integrated guided mode filter," Electron. Lett. **48**, 1619–1621 (2012).
9. K. Chan Shin Yu and A. -. Fehrembach and O. Gauthier-Lafaye and A. Monmayrant and S. Bonnefont and P. Arguel and F. Lozes-Dupuy and A. Sentenac, "Design of a mid infrared resonant grating filter," CAS 2010 Proceedings (International Semiconductor Conference) **01**, 151–154 (2010).
10. N. Rassem, E. Popov, and A.-L. Fehrembach, "Numerical modeling of long sub-wavelength patterned structures," Opt. Quantum Electron. **47**, 3171–3180 (2015).
11. S. Pelloquin, S. Augé, K. Sharshavina, J.-B. Doucet, A. Héliot, H. Camon, A. Monmayrant, and O. Gauthier-Lafaye, "Soft mold nanoimprint lithography: a versatile tool for sub-wavelength grating applications," Microsystem Technologies, in press (2018).
12. A. Yariv, "Universal relations for coupling of optical power between microresonators and dielectric waveguides," Electron. Lett. **36**, 321 (2000).

#338375 https://doi.org/10.1364/OE.26.027014
Journal © 2018 Received 13 Jul 2018; revised 13 Sep 2018; accepted 13 Sep 2018; published 2 Oct 2018

Optics EXPRESS

1. Introduction

Cavity Resonator Integrated Grating Filters (CRIGFs) are spectrally narrow and efficient reflective filters [1] derived from the more widespread guided modes resonant filters (GMRFs) [2]. They both rely on grating coupler (GC) to couple free-space waves to a guided mode inside a planar waveguide and exhibit Fano spectral resonance when Bragg coupling conditions are met.

CRIGFs and GMRFs differ in that the GC in the CRIGF is usually few-periods-long and enclosed between two side Distributed Bragg Reflectors (DBRs) (see Fig. 1) thus forming a cavity, while the GC in the GMRF is long and unbounded and can be considered infinite in most cases. Those different geometries create different kinds of modes: the modes in a GMRF are propagating leaky guided-modes, while the modes in a CRIGF are lossy Fabry-Perot cavity modes [3, 4]. As a result, GMRFs have extremely low angular tolerance whereas CRIGFs show unprecedented angular tolerance [5] and the position of the spectral resonance of a GMRF can be tuned with the angle of incidence while that of a CRIGF is unaffected.

So far, CRIGFs have only been developed in the NIR, in particular for inter-chip communication [6, 7] and for the design of compact and robust extended cavity diode laser [8] where they act both as a wavelength selective element and a cavity end mirror. CRIGFs with resonances in the mid-infrared (MIR) would be particularly interesting to frequency stabilize quantum cascade laser diodes. In this paper, we demonstrate experimentally CRIGFs working in the mid-infrared ($\simeq 2200$ cm^{-1}) that were fabricated for this purpose. Extension of CRIGFs to this spectral range requires challenging design, fabrication and optical characterization that are detailed hereafter.

2. Design and simulation

To design and fabricate CRIGFs in the MIR, we usually rely on the GaAs/AlAs system. Three reasons support this choice. First, it is a mature material system providing high quality transparent materials in the whole MIR range, nominally [1-12] μm range. Second, multilayer coatings can be designed alternating GaAs and high Al content $Al_xGa_{1-x}As$ layers, with optical index contrasts of up to 0.4, and layer deposition is extremely precise and homogeneous when they are fabricated by epitaxial growth. Last, mature optoelectronic micro- and nano- processes are easily available for sample fabrication. However, as compared to material systems available for the visible (like Si_3N_4/SiO_2) or the NIR (like SiO_2/Si) GaAs/AlAs offers a reduced relative index contrast while both GaAs and AlAs have fairly high optical indices. This introduces specific challenges when designing a CRIGF with this material [9]. First, the structure relies on a GaAs high-optical-index substrate which complicates the design of the low-loss waveguide inherent to CRIGF structures. A thick buffer layer is usually required to isolate the waveguide from the substrate and reduce losses. Second, as with standard GMRF the sidebands reflectivity is fixed by the overall reflectivity of the multilayer stack. Thus designing an antireflection coating with only a few layers (to achieve a single mode waveguide and maintain a relatively low thickness of the stack for practicability issues) using only high index GaAs and AlAs materials is challenging. As a consequence, the resulting antireflection is usually less efficient and more narrowband than what can be achieved in the visible and NIR spectral ranges.

An optimized structure of CRIGF based on GaAs/AlAs is presented on Fig. 1. A partially-etched top GaAs layer serves both as a waveguide and as Distributed Bragg Reflectors (DBR) and Grating Coupler (GC). It rests upon a thick AlAs layer to prevent leakage of the guided modes into the high index-GaAs substrate. An infinitely large GC is first optimized to provide a sharp spectral peak at the desired wavelength (4.6 μm) and an antireflection around it for TE polarization. This sets the layers thickness (see Fig. 1), the grating depth (0.54 μm), filling factor ($f_{GC} = 0.85$) and period ($\Lambda_{GC} = 1.46\,\mu$m). The DBR period is set to $\Lambda_{DBR} = \Lambda_{GC}/2$ and its filling factor to $f_{DBR} = 0.5$ to maximize its efficiency at the resonant wavelength. In a last step we manually optimize the lengths L_{DBR} of the DBR, L_{GC} of the GC, and of L_{PS} the

Optics EXPRESS

phase shift sections. This numerical modelling of the CRIGF is done with a home-made code based on the Fourier Modal Method using the super-cell technique and the decomposition of the incident gaussian beam over the numerous diffraction orders of the structure [10]. This allows the calculation of the reflectivity of the CRIGF when illuminated by a gaussian beam.

However, we could not fabricate the resulting optimized structure. Indeed, the AlAs buffer is too thick to be grown ontop of the GaAs substrate (see section 3). We thus had to replace it by a $Ga_{0.1}Al_{0.9}As$ buffer layer (see Fig. 1). As this new buffer have a higher refractive index than AlAs, its thickness was slightly reduced from 5.70 μm down to 5.61 μm in order to keep the optical thickness constant. The consequence of this change is twofold: first, the overall structure was not completely re-optimized for this new material system, resulting in slightly reduced performance; second, the refractive index contrast is reduced, decreasing the efficiency and bandwidth of the background anti-reflection.

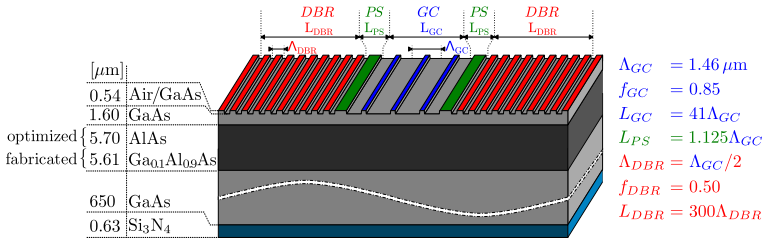

Fig. 1. MIR CRIGF schematic, with side DRBs (red), phase shifting sections (PS, green) and central grating coupler (GC, blue). The structures as optimized numerically and as fabricated only differ by the composition and thickness of the low-index buffer layer.

The reflectivity of this structure based on GaAs/$Ga_{0.1}Al_{0.9}As$ was simulated (see Fig. 2) for a TE-polarized incident gaussian beam (electric-field aligned with the grating grooves). A peak reflectivity of 81% and a Q factor of 1200 are obtained around 4.71 μm. This resonant wavelength is slightly different from the target one (4.61 μm) but it can be adjusted by changing the GC periodicity Λ_{GC}.

3. Sample fabrication

The first fabrication step is the growth of the vertical stack by molecular beam epitaxy (MBE) on a GaAs substrate. Due to lattice mismatch, growing 5.70 μm of AlAs on GaAs for the optimized structure resulted in many defects and the heterostructure was not stable. We thus changed the structure and grew 5.61 μm of $Ga_{0.1}Al_{0.9}As$ capped with a 2.14 μm GaAs top layer. After MBE growth, the sample was capped with a 100-nm-thick SiO_2 layer for use as a hard mask for dry etching. The CRIGF patterns were defined on a silicon hard mold by step and repeat photolithography using a Canon 3000i4 with 5× size reduction, and then transfered onto the SiO_2 hard mask on the GaAs sample by soft-mold UV-nanoimprint lithography and fluorinated dry etching [11]. Eventually, the patterns were etched 540-nm-deep in the GaAs top layer using ICP-RIE (Inductively-Coupled-Plasma Reactive-Ion-Etching) dry etching. A final selective CF_4/O_2 plasma etching allowed to remove the residual SiO_2 hard mask. As a final step a 0.63 μm-thick Si_3N_4 anti-reflection layer was deposited by ICP-PECVD (Inductively-Coupled-Plasma Plasma-Enhanced-Chemical-Vapor-Deposition) on the backside of the substrate.

An array of the CRIGFs with varying parameters was fabricated on each sample. The central GC is made of 41 periods Λ_{GC}, where $\Lambda_{GC} = 1.44, 1.46$ or $1.48\,\mu$m. Each side of the GC is flanked with a phase section PS of length $L_{PS} = [1.000, 1.125$ or $1.300] \times \Lambda_{GC}$ and a DBR with 300 periods with a filling factor of 0.5 and a periodicity $\Lambda_{DBR} = \Lambda_{GC}/2$.

The Fig. 2(b) shows a Focused Ion Beam Etching (FIBE) cut of the sample. On this figure the

Optics EXPRESS

top layer of GaAs is covered by a platinum layer (Pt) as part of the FIBE process. This Pt layer is not present in the final sample. Last, the fabricated samples were cleaved and reported on an aluminum sub-mount for characterization.

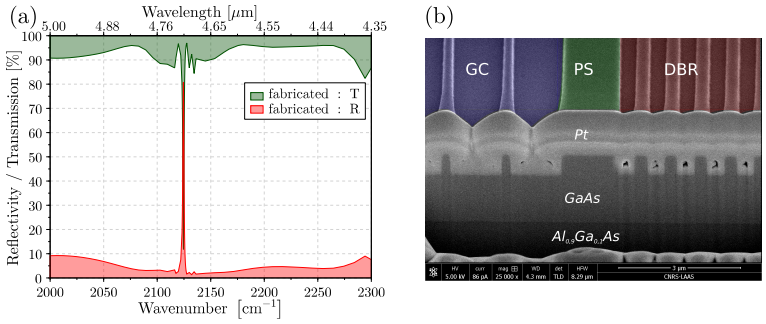

Fig. 2. (a) Calculated spectral reflection (red) and transmission (green) for the fabricated structure; (b) FIBE cut of the fabricated sample. The top platinum layer (Pt) is added during the cut and is not part of the final sample.

4. Optical characterization and results

We use a standard FTIR spectrometer Nicolet 6700 equipped with a MCT-A detector operating at liquid nitrogen temperature. The spectrometer is coupled to Continuum infrared microscope operated in reflectivity regime. The later is equipped with ZnSe infrared focusing objectives that allow the collection of reflected infrared signal in a narrow angular range close to normal incidence while providing high transmission and almost constant refractive index from 4 μm (2500 cm^{-1}) to 5 μm (2000 cm^{-1}). We used three ZnSe focusing objectives with 6-mm, 12-mm, and 18-mm focal lengths corresponding to maximum collection half-angles of 14.5°, 7.5°, and 4.5°, respectively. The reflected signal can be also collected in transverse magnetic (TM) and transverse electric (TE) polarization by using a KRS-5 holographic wire grid infrared polarizer providing excellent transmission in the working frequency range. We use a Globar heat radiation source and modulate its infrared emission with the Michelson interferometer of the spectrometer.

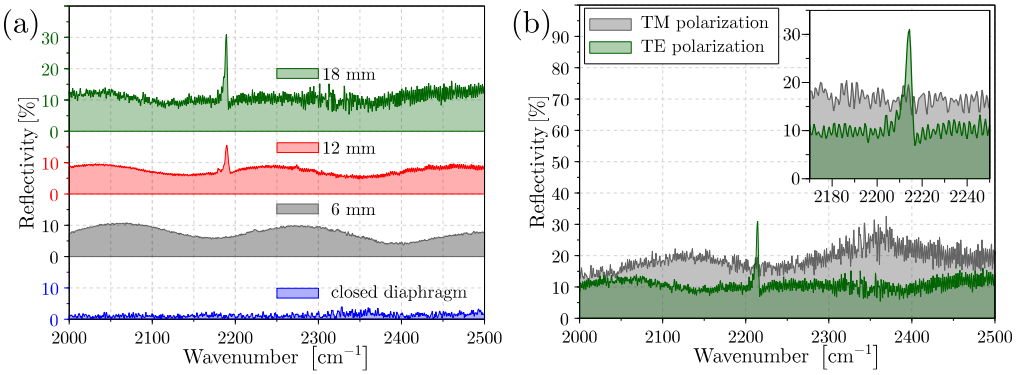

Fig. 3. (a) Experimental spectral reflectivity of the same CRIGF, under TE illumination, for the 3 refractive objectives 18 mm (green), 12 mm (red), 6 mm (gray) together with a reference for a closed diaphragm (blue); (b) Experimental spectral reflectivity for TM-polarized (gray) and TE-polarized (green) incident beam using the 18-mm objective. The CRIGF is designed for TE polarization. Inset: zoom on the resonant peak. For both (a) and (b), the CRIGF geometry is $\Lambda_{GC} = 1.44$ μm, $f_{GC} = 0.72$, $L_{PS} = 1.125 \times \Lambda_{GC}$.

Optics EXPRESS

As seen in Fig. 3(a), the measurement of the spectral reflectivity of CRIGF with a FTIR is particularly tricky. Indeed, for short-focal-lengths objective, the high numerical aperture gives a high signal to noise ratio and an accurate measurement of the slowly-varying out-of-resonance reflectivity (gray and red curves). However, the sharp spectral peak is only detectable for long-focal-length objectives (green curve) with reduced numerical aperture and signal to noise ratio. Indeed, the CRIGFs under study have a limited angular acceptance corresponding to a half-angle of 2.2°. The 3 available objectives have higher numerical apertures, and thus part of the illumination is out of the angular acceptance of the CRIGF and the peak reflectivity is underestimated. The best measurement is obtained with the lowest numerical aperture available (18-mm objective, green curve in Fig. 3(a)) but it is still twice bigger than the optimal one (4.5° vs 2.2°) and we thus believe that the measured peak reflectivity could be greatly improved using a longer-focal-length objective.

Following these first experimental observations, the measurements were normally performed with the 18-mm objective, a spectral resolution of 1 cm^{-1} averaged over 256 scans with the polarizer selecting TE illumination conditions. The alignment of the sample is performed for visible wavelength and then adjusted for infrared range to compensate for ZnSe chromatic aberrations. The collection spot on the sample was set to be smaller than the GC and was not exceeding 50 μm in diameter.

We first characterized the polarization dependence of the reflectivity of the filter (Fig. 3(b)). As expected, a peak in the spectral reflectivity only occurs for the designed polarization (TE). This peak reaches 30% for a Q factor of 600. Moreover, the background reflectivity, albeit fairly high for both polarizations, is noticeably higher when the wrong polarization (TM) is used, showing that the polarization dependent antireflection multistack is somewhat effective. However, it is higher than expected from the simulation, most probably because the reflectivity peaks from the CRIGFs do not lie exactly within the narrow spectral region of low reflectivity provided by the multistack (see Fig. 2(a)).

We then studied the impact of the length of the phase-shift section L_{PS} and found an optimum for $L_{PS} = 1.125 \times \Lambda_{GC}$ in agreement with simulations and previous studies on NIR CRIGFs [3]. For the rest of the experiments, we focus on CRIGFs with $L_{PS} = 1.125 \times \Lambda_{GC}$.

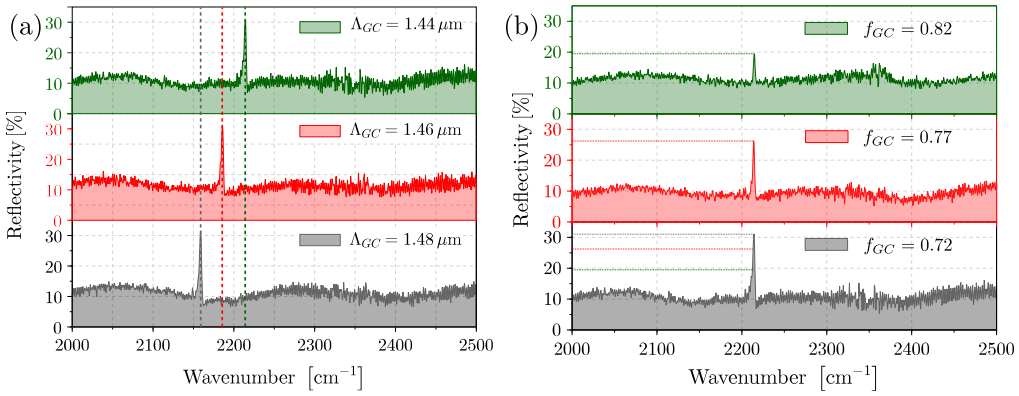

Fig. 4. (a) Experimental spectral reflectivity for 3 CRIGFs with respective base period of 1.44, 1.46 and 1.48μm ($f_{GC} = 0.72$, $L_{PS} = 1.125 \times \Lambda_{GC}$); (b) Experimental spectral reflectivity for 3 CRIGFs with varying filling factors of the grating coupler. The CRIGF geometry is $\Lambda_{GC} = 1.44\,\mu$m, $L_{PS} = 1.125 \times \Lambda_{GC}$. The 18-mm objective was used.

As shown in Fig. 4(a), the resonant peak can be tuned linearly by changing the base period of the CRIGF (Λ_{GC}), the out of resonance reflectivity remaining unchanged. For a given Λ_{GC}, the experimental resonant wavelength is slightly lower than the calculated one. This is most probably

Optics EXPRESS

due to an effective index inside the CRIGF cavity slightly lower than expected.

We studied 3 CRIGFs with varying filling factors for the grating coupler: $f_{GC} = 0.72$, 0.77 and 0.82. As seen in Fig. 4(b), the highest experimental reflectivity (30%) is obtained for a filling factor of $f_{GC} = 0.72$. It corresponds to the smallest filling factor coded on the sample and reflectivities beyond 30% might be obtained for smaller values of the filling factor. This variation of the maximum reflectivity with the filling factor is not predicted by our simulations which do not take losses into account and the filling factor of 0.85 was chosen mainly to minimize the reflectivity out of resonance.

Our understanding of this effect is the following. The closer the filling factor to 0.5, the stronger the coupling between the cavity mode inside the CRIGF and the incoming beam. The coupling needs to be matched to the intrinsic losses of the cavity in order to maximize the reflectivity (similarly to the critical coupling condition in absorbers) [12]. The fact that the optimum reflectivity occurs for filling factors close to 0.5 and thus for high coupling coefficients, together with reduced Q factor are strong indicators that the cavity inside the CRIGF is lossier than expected. These losses could have several origins. First, propagation losses could be induced by absorption in the materials or diffusion due to oval defects or imperfection and roughness on the grating profile. Such losses are not taken into account in our simulations. Second, other propagation losses may be due to higher leakage of the guided mode into the high index GaAs substrate. This leakage is highly dependent on the thickness and optical index of the buffer layer and may be underestimated in our simulation. Last, the side DBRs might be less effective then expected, in particular owing to stitch field errors during the reticle fabrication for optical lithography. Such errors are known to reduce the efficiency of the distributed reflection, and each DBR is 5 times longer than the field of the equipment we used for mask fabrication.

Last, we studied the spatial dependence of the reflectivity by moving the sample under the illumination spot and plotting the reflectivity at the resonant wavelength versus sample coordinate, resulting in a spatial mapping of the reflectivity (Fig. 5). The resonant reflectivity is well localized within the central part of the CRIGF (GC) and corresponds to a small area of around $60 \times 100\ \mu m^2$, confirming the localized origin of the resonance, in good agreement with [3].

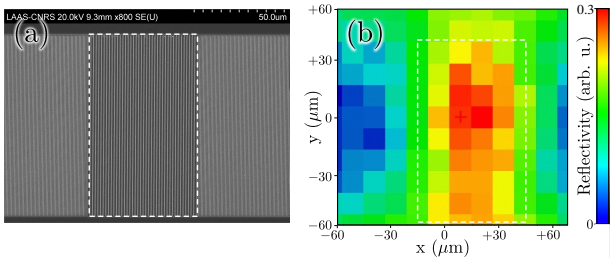

Fig. 5. (a) SEM image of the sample and (b) map of the spatial reflectivity showing a localized mode under the grating coupler of the CRIGF (the white dashed rectangle is a guide to the eye for the grating coupler boundaries).

5. Conclusion

We demonstrated experimentally Cavity Resonator Integrated Grating Filters (CRIGFs) working in the MIR. This result in the fabrication and demonstration of several small-area filters, with Q-factor around 600 and peak resonance between 2160 and 2215 cm^{-1}. The maximum measured peak reflectivity of around 30 % might be underestimated due to the incoherent illumination inherent to FTIR that does not necessarily match the numerical aperture required for the CRIGFs under study. This peak reflectivity might be increased by a better matching of numerical aperture of the designed CRIGFs to that of the FTIR. These components exhibit narrow spectral reflectivity

Optics EXPRESS

and localized field enhancement which could be useful in spectroscopic or sensing applications or for wavelength stabilization of semiconductor lasers such as quantum cascade laser diodes.

Funding

S. Augé acknowledges financial support from DGA and Centre National d'Etudes Spatiales (CNES) PhD grants under the supervision of P. Adam and B. Faure. We acknowledge financial support from Agence Nationale de la Recherche under grant ANR14-ASTR-0024-01.

Acknowledgments

Authors thankfully acknowledge the LAAS clean room team for technical support and technological expertise provided within the French RENATECH framework.